

Architectures for Long-Distance Quantum Communication

Jeffrey H. Shapiro

Research Laboratory of Electronics

Massachusetts Institute of Technology, Cambridge, MA 02139

Abstract

A quantum communication system that is capable of long-distance, high-fidelity teleportation, and long-duration quantum storage is proposed. This system uses polarization-entangled photons and trapped-atom quantum memories and is compatible with transmission over standard telecommunication fiber. An extension of this architecture permits long-distance transmission and storage of Greenberger-Horne-Zeilinger states.

I. INTRODUCTION

The preeminent obstacle to the development of quantum information technology is the difficulty of transmitting quantum information over noisy and lossy quantum communication channels, recovering and refreshing the quantum information that is received, and then storing it in a reliable quantum memory. A team of researchers from the Massachusetts Institute of Technology and Northwestern University (MIT/NU) is developing a singlet-based quantum communication approach [1] that uses a novel ultrabright source of polarization-entangled photon pairs [2], and a trapped-atom quantum memory [3] whose loading can be nondestructively verified and whose structure permits all four Bell-state measurements to be performed. This paper reviews the primitives for the MIT/NU architecture. A loss-limited-performance analysis shows that this architecture can achieve a throughput as high as 500 entangled-pairs/sec with 95% fidelity over a 50 km path when there is 10 dB of fixed loss in the overall system and 0.2 dB/km of propagation loss in the fiber. An additional primitive—the type-II degenerate optical parametric amplifier (OPA)—is then introduced. This source, which is less complicated than the dual-OPA arrangement from [2], is somewhat less effective in long-distance singlet-state teleportation. It can be used, however, within the MIT/NU architecture to perform long-distance transmission and storage of Greenberger-Horne-Zeilinger (GHZ) states via an alerted detection system akin to that in [4]. The addition of a heralded single-photon source primitive can be used to both eliminate the need for alerted detection in this GHZ-state transmission scheme, and to greatly increase its throughput.

II. LONG-DISTANCE TELEPORTATION

The notion that singlet states could be used to achieve teleportation is due to Bennett *et al.* [5]. The transmitter and receiver stations share the entangled qubits of a singlet state

and the transmitter then accepts an input-mode qubit. Making the Bell-state measurements on the joint input-mode/transmitter system then yields the two bits of classical information that the receiver needs to reconstruct the input state. An initial experimental demonstration of teleportation using singlet states was performed by Bouwmeester *et al.* [6,7], but only one of the Bell states was measured, the demonstration was a table-top experiment, and it did not include a quantum memory. Our proposal for a singlet-based quantum communication system, which is shown in Fig. 1, remedies all of these limitations.



FIG. 1. Schematic of long-distance quantum communication system: P = ultrabright narrowband source of polarization-entangled photon pairs; L = L km of standard telecommunication fiber; M = trapped-atom quantum memory.

An ultrabright narrowband source of polarization-entangled photon pairs [2] launches the entangled qubits from a singlet state into two L -km-long standard telecommunication fibers. The photons emerging from the fibers are then loaded into trapped-atom quantum memories [3]. These memories store the photon-polarization qubits in long-lived hyperfine levels. Because it is compatible with fiber-optic transmission, this configuration is capable of long-distance teleportation. Because of the long decoherence times that can be realized with trapped atoms, this configuration supports long-duration quantum storage. We devote the rest of this section to summarizing the basic features of our proposal.

Each M block in Fig. 1 is a quantum memory in which a single ultra-cold ^{87}Rb atom (~ 6 MHz linewidth) is confined by a CO_2 -laser trap in an ultra-high vacuum chamber with cryogenic walls within a high-finesse (~ 15 MHz linewidth) single-ended optical cavity. This memory can absorb a 795 nm photon, in an arbitrary polarization state, transferring the qubit from the photon to the degenerate B levels of Fig. 2(a) and thence to long-lived storage levels, by coherently driving the B -to- D transitions. (We are using abstract symbols here for the hyperfine levels of rubidium, see [3] for the actual atomic levels involved as well as a complete description of the memory and its operation.) With a liquid helium cryostat, so that the background pressure is less than 10^{-14} Torr, the expected lifetime of the trapped rubidium atom will be more than an hour. Fluctuations in the residual magnetic field, however, will probably limit the atom's decoherence time to a few minutes. By using optically off-resonant Raman (OOR) transitions, the Bell states of two atoms in a single vacuum-chamber trap can be converted to superposition states of one of the atoms. All four Bell measurements can then be made, sequentially, by detecting the presence (or absence) of fluorescence as an appropriate sequence of OOR laser pulses is applied to the latter atom. The Bell-measurement results in one memory can be sent to a distant memory, where at most two additional OOR pulses are needed to complete the Bennett *et al.* state transformation. The qubit stored in a trapped rubidium atom can be converted back into a photon by reversing the Raman excitation process that occurs during memory loading.

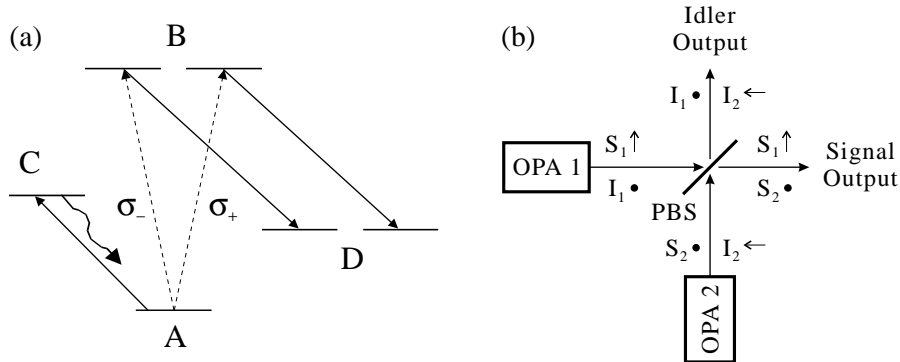


FIG. 2. Essential components of singlet-state quantum communication system from Fig. 1. Left (a), simplified atomic-level schematic of the trapped rubidium atom quantum memory: A -to- B transition occurs when one photon from an entangled pair is absorbed; B -to- D transition is coherently driven to enable storage in the long-lived D levels; A -to- C cycling transition permits nondestructive determination of when a photon has been absorbed. Right (b), ultrabright narrowband source of polarization-entangled photon pairs: each optical parametric amplifier (OPA1 and OPA2) is type-II phase matched; for each optical beam the propagation direction is \hat{z} , and \hat{x} and \hat{y} polarizations are denoted by arrows and bullets, respectively; PBS, polarizing beam splitter.

The P -block in Fig. 1 is an ultrabright narrowband source of polarization-entangled photon pairs, capable of producing $\sim 10^6$ pairs/sec in ~ 30 MHz bandwidth by appropriately combining the signal and idler output beams from two doubly-resonant type-II phase-matched optical parametric amplifiers (OPAs), as sketched in Fig. 2(b) [2]. The fluorescence spectrum of the signal and idler beams is controlled by the doubly-resonant OPA cavities. These can be advantageously and easily tailored to produce the desired (factor-of-two broader than the memory-cavity's) bandwidth. By using periodically-poled potassium titanyl phosphate (PPKTP), a quasi-phase-matched type-II nonlinear material, we can produce $\sim 10^6$ pairs/sec at the 795 nm wavelength of the rubidium memory for direct memory-loading (i.e., local-storage) applications. For long-distance transmission to remotely-located memories, we use a different PPKTP crystal and pump wavelength to generate $\sim 10^6$ pairs/sec in the 1.55- μm -wavelength low-loss fiber transmission window. After fiber propagation we then shift the entanglement to the 795 nm wavelength needed for the rubidium-atom memory via quantum-state frequency translation [8,9].

Successful singlet transmission requires that polarization not be degraded by the propagation process. Our scheme for polarization maintenance relies on time-division multiplexing. Time slices from the signal beams from our two OPAs are sent down one fiber in the same linear polarization but in nonoverlapping time slots, accompanied by a strong out-of-band laser pulse. By tracking and restoring the linear polarization of the strong pulse, we can restore the linear polarization of the signal-beam time slices at the far end of the fiber. After this linear-polarization restoration, we then reassemble a time-epoch of the full vector signal beam by delaying the first time slot and combining it on a polarizing beam splitter with the second time slot after the latter has had its linear polarization rotated by 90° . A similar

procedure is performed to reassemble idler time-slices after they have propagated down the other fiber in Fig. 1. This approach, which is inspired by the Bergman *et al.* two-pulse fiber-squeezing experiment [10], common-modes out the vast majority of the phase fluctuations and the polarization birefringence incurred in the fiber, permitting standard telecommunication fiber to be used in lieu of the lossier and much more expensive polarization-maintaining fiber.

III. LOSS-LIMITED PERFORMANCE

Quantum communication is carried out in the Fig. 1 configuration via the following protocol. The entire system is clocked. Time slots of signal and idler (say 400 ns long) are transmitted down optical fibers to the quantum memories. These slots are gated into the memory cavities—with their respective atoms either physically displaced or optically detuned so that no *A-to-B* (i.e., no 795 nm) absorptions occur. After a short loading interval (a few cold-cavity lifetimes, say 400 ns), each atom is moved (or tuned) into the absorbing position and *B-to-D* coherent pumping is initiated. After about 100 ns, coherent pumping ceases and the *A-to-C* cycling transition [shown in Fig. 2(a)] is repeatedly driven (say 30 times, taking nearly 1 μ s). By monitoring a cavity for the fluorescence from this cycling transition, we can reliably detect whether or not a 795 nm photon has been absorbed by the atom in that cavity. If neither atom or if only one atom has absorbed such a photon, then we cycle both atoms back to their *A* states and start anew. If no cycling-transition fluorescence is detected in either cavity, then, because we have employed enough cycles to ensure very high probability of detecting that the atom is in its *A* state, it must be that both atoms have absorbed 795 nm photons and stored the respective qubit information in their long-lived degenerate *D* levels. These levels are not resonant with the laser driving the cycling transition, and so the loading of our quantum memory is nondestructively verified in this manner.

We expect that the preceding memory-loading protocol can be run at rates as high as $R = 500$ kHz, i.e., we can get an independent try at loading an entangled photon pair into the two memory elements of Fig. 1 every 2 μ s. With a high probability, P_{erasure} , any particular memory-loading trial will result in an erasure, i.e., propagation loss and other inefficiencies combine to preclude both atoms from absorbing photons in the same time epoch. With a small probability, P_{success} , the two atoms will absorb the photons from a single polarization-entangled pair, viz., we have a memory-loading success. With a much smaller probability, P_{error} , both atoms will have absorbed photons but these photons will not have come from a single polarization-entangled pair; this is the error event.

There are two key figures-of-merit for the Fig. 1 configuration: throughput and fidelity. Propagation losses and other inefficiencies merely increase P_{erasure} and hence reduce the throughput, i.e., the number of successful entanglement-loadings/sec, $N_{\text{success}} \equiv RP_{\text{success}}$, that could be achieved if the quantum memories each contained a lattice of trapped atoms for sequential loading of many pairs. Loading errors, which occur with probability P_{error} , provide the ultimate limit on the teleportation fidelity that can be realized with the Fig. 1 architecture. This loss-limited fidelity is given by $F_{\text{max}} = 1 - P_{\text{error}}/2(P_{\text{success}} + P_{\text{error}})$, where we have assumed that the error event loads independent, randomly-polarized photons into

each memory.

A. OPA Statistics

Assume matched signal and idler cavities, each with linewidth Γ , zero detuning, and no excess loss. Also assume anti-phased pumping at a fraction, G^2 , of oscillation threshold, with no pump depletion or excess noise. From [2] we then have that the output beams from OPAs 1 and 2 are in an entangled, zero-mean Gaussian pure state, which is completely characterized by the following normally-ordered and phase-sensitive correlation functions:

$$\langle \hat{A}_{k_j}^\dagger(t + \tau) \hat{A}_{k_j}(t) \rangle = \frac{G\Gamma}{2} \left[\frac{e^{-(1-G)\Gamma|\tau|}}{1-G} - \frac{e^{-(1+G)\Gamma|\tau|}}{1+G} \right], \quad (3.1)$$

$$\langle \hat{A}_{S_j}(t + \tau) \hat{A}_{I_j}(t) \rangle = \frac{(-1)^{j-1}G\Gamma}{2} \left[\frac{e^{-(1-G)\Gamma|\tau|}}{1-G} + \frac{e^{-(1+G)\Gamma|\tau|}}{1+G} \right], \quad (3.2)$$

where $\{ \hat{A}_{k_j}(t)e^{-i\omega_k t} : k = S \text{ (signal), } I \text{ (idler), } j = 1, 2 \}$ are positive-frequency, photon-units OPA-output field operators. The presence of excess loss within the OPA cavities, and/or propagation loss along the fiber can be incorporated into this OPA analysis in a straightforward manner [11]. Assuming symmetric operation, in which the signal and idler encounter identical intracavity and fiber losses, then the correlation-function formulas, Eqs. (3.1) and (3.2), are merely multiplied by $\eta_L\gamma/\Gamma$, where $\eta_L < 1$ is the transmission through the fiber and $\gamma < \Gamma$ is the output-coupling rate of the OPA cavity.

B. Cavity-Loading Statistics

The internal annihilation operators of the quantum memory cavities—over the T_c -sec-long loading interval—are related to the incoming signal and idler field operators as follows:

$$\hat{a}_k(T_c) = \hat{a}_k(0)e^{-\Gamma_c T_c} + \int_0^{T_c} dt e^{-\Gamma_c(T_c-t)} \left[\sqrt{2\gamma_c} \tilde{A}_k(t) + \sqrt{2(\Gamma_c - \gamma_c)} \tilde{A}_{k_v}(t) \right], \quad (3.3)$$

for $k = S, I$, where $\gamma_c < \Gamma_c$ is the input-coupling rate and Γ_c is the linewidth of the (assumed to be identical for signal and idler) memory cavities. The initial intracavity operators and the loss-operators, $\{ \hat{a}_k(0), \tilde{A}_{k_v}(t) \}$, are in vacuum states.

It is now easy to show that the joint density operator (state) for $\{ \hat{a}_S(T_c), \hat{a}_I(T_c) \}$, takes the factored form, $\hat{\rho}_{\vec{S}\vec{I}} = \hat{\rho}_{S_x I_y} \hat{\rho}_{S_y I_x}$, where the two-mode density operators on the right-hand side are Gaussian mixed states given by the anti-normally ordered characteristic functions,

$$\begin{aligned} \text{tr} \left[\hat{\rho}_{S_x I_y} e^{-\zeta_S^* \hat{a}_{S_x} - \zeta_I^* \hat{a}_{I_y}} e^{\zeta_S \hat{a}_{S_x}^\dagger + \zeta_I \hat{a}_{I_y}^\dagger} \right] &= \text{tr} \left[\hat{\rho}_{S_y I_x} e^{-\zeta_S^* \hat{a}_{S_y} + \zeta_I^* \hat{a}_{I_x}} e^{\zeta_S \hat{a}_{S_y}^\dagger - \zeta_I \hat{a}_{I_x}^\dagger} \right] \\ &= e^{-(1+\bar{n})(|\zeta_S|^2 + |\zeta_I|^2) + 2\bar{n}\text{Re}(\zeta_S \zeta_I)}, \end{aligned} \quad (3.4)$$

where $\bar{n} \equiv I_- - I_+$ and $\tilde{n} \equiv I_- + I_+$, with $I_\mp \equiv \eta_L \gamma \gamma_c G / \Gamma_c (1 \mp G) [(1 \mp G)\Gamma + \Gamma_c]$.

C. Throughput and Fidelity Calculations

From the loaded-cavity state we can find the erasure, success, and error probabilities via,

$$P_{\text{erasure}} = ({}_{S_x}\langle 0|\hat{\rho}_{S_x}|0\rangle_{S_x}) ({}_{S_y}\langle 0|\hat{\rho}_{S_y}|0\rangle_{S_y}) + ({}_{I_x}\langle 0|\hat{\rho}_{I_x}|0\rangle_{I_x}) ({}_{I_y}\langle 0|\hat{\rho}_{I_y}|0\rangle_{I_y}) \\ - ({}_{S_x}\langle 0|{}_{I_y}\langle 0|\hat{\rho}_{S_x I_y}|0\rangle_{I_y}|0\rangle_{S_x}) ({}_{S_y}\langle 0|{}_{I_x}\langle 0|\hat{\rho}_{S_y I_x}|0\rangle_{I_x}|0\rangle_{S_y}), \quad (3.5)$$

$$P_{\text{success}} = {}_{\text{SI}}\langle \psi|\hat{\rho}_{\bar{S}\bar{I}}|\psi\rangle_{\text{SI}} \quad \text{and} \quad P_{\text{error}} = 1 - P_{\text{erasure}} - P_{\text{success}}, \quad (3.6)$$

where $|\psi\rangle_{\text{SI}} \equiv (|1\rangle_{S_x}|1\rangle_{I_y}|0\rangle_{S_y}|0\rangle_{I_x} - |0\rangle_{S_x}|0\rangle_{I_y}|1\rangle_{S_y}|1\rangle_{I_x})/\sqrt{2}$, is the singlet state.

In Fig. 3(a) we have plotted the throughput of our quantum communication system when, for every path length, the OPA gain is adjusted to maximize N_{success} under the fidelity constraint $F_{\text{max}} = 0.95$. The following parameter values are assumed: 5 dB of excess loss in each P -to- M block path in Fig. 1; 0.2 dB/km loss in each fiber; $\Gamma_c/\Gamma = 0.5$; and $R = 500$ kHz memory cycling rate. We see from this figure that a throughput of 500 pairs/sec can be sustained out to an end-to-end path length ($2L$) of 50 km while maintaining a loss-limited fidelity of 95%. Figure 3(b) shows that the pumping required for this performance is quite modest; 2–3% of oscillation threshold suffices.

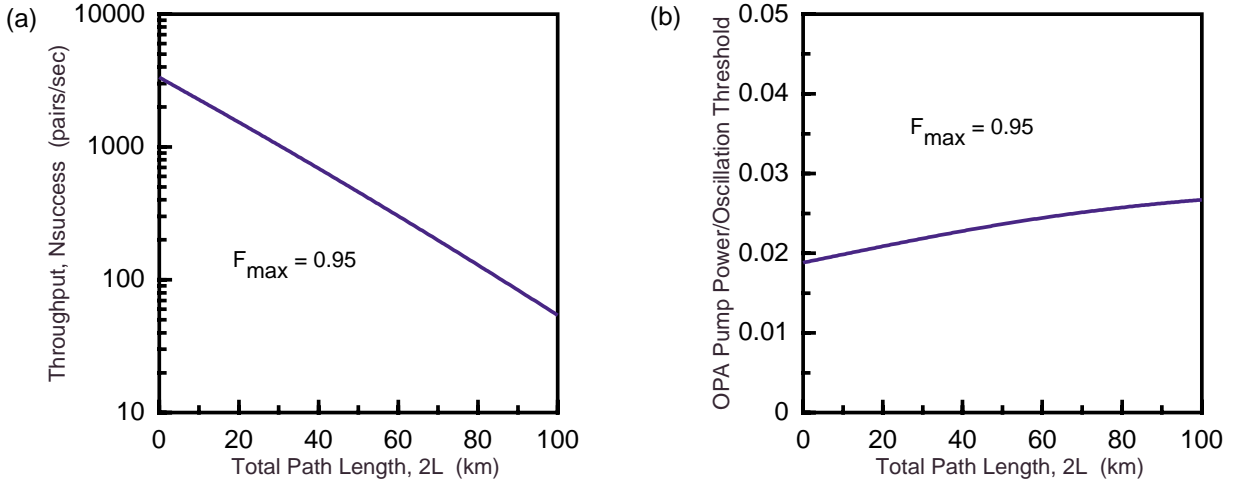


FIG. 3. Gain-optimized performance of the Fig. 1 architecture. Left (a), optimized throughput, N_{success} , vs. total path length, $2L$, at 95% limiting entanglement fidelity, F_{max} . Right (b), normalized OPA gain G^2 vs. total path length, $2L$, needed to realize this optimized throughput. Both curves assume 5 dB of excess loss per P -to- M block connection, and 0.2 dB/km fiber-propagation loss.

IV. TELEPORTATION WITH A DEGENERATE PARAMETRIC AMPLIFIER

The singlet-state teleportation architecture that we have just described relies on a pair of coherently-pumped optical parametric amplifiers for its entangled photons. It turns out

that a simpler source arrangement offers comparable quantum communication performance. Consider the doubly-resonant, type-II phase matched degenerate parametric amplifier shown schematically in Fig. 4.

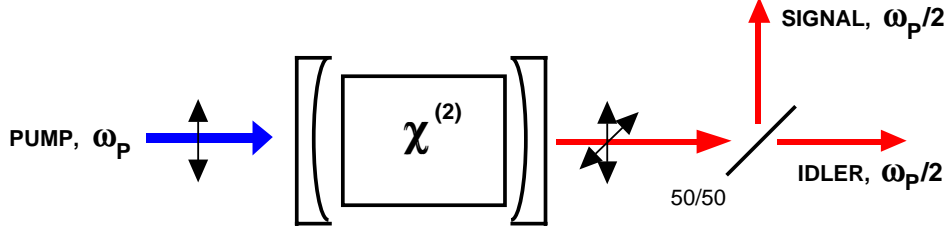


FIG. 4. Doubly-resonant, type-II phase matched degenerate optical parametric amplifier. Signal and idler photons emerge in frequency-degenerate, orthogonally-polarized pairs from the OPA cavity. The joint state of the beams exiting the 50/50 beam splitter is mixed, but includes a triplet component that can be used as the entanglement source in the Fig. 1 teleportation architecture.

Operated at degeneracy, the center frequencies of the signal and idler beams exiting the OPA cavity are both equal to $\omega_P/2$, i.e., half the OPA's pump frequency. Because the OPA produces signal and idler photons in pairs, and the members of each pair are distinguishable only because of their orthogonal polarizations, the 50/50 beam splitter in Fig. 4 yields output beams containing a triplet-state component. In particular, when a signal/idler pair encounters this beam splitter there is a 50/50 chance that one photon will appear in each output port. When this occurs, a symmetry argument shows that the joint output state from the 50/50 beam splitter is $|\phi\rangle_{SI} \equiv (|1\rangle_{S_x}|1\rangle_{I_y}|0\rangle_{S_y}|0\rangle_{I_x} + |0\rangle_{S_x}|0\rangle_{I_y}|1\rangle_{S_y}|1\rangle_{I_x})/\sqrt{2}$. A simple modification can be made to the Bennett *et al.* teleportation protocol so that this triplet can be used in lieu of the singlet state.

If the degenerate-OPA arrangement from Fig. 4 is used as the source block in the Fig. 1 architecture, the OPA statistics, cavity-loading statistics, and throughput/fidelity calculations from Sect. III can easily be adapted to this new configuration. In particular, the joint density operator for $\{\tilde{a}_S(T_c), \tilde{a}_I(T_c)\}$ is a Gaussian mixed state that is given by the following anti-normally ordered characteristic function,

$$\text{tr} \left[\hat{\rho}_{S_x I_x S_y I_y} e^{-\zeta_{S_x}^* \hat{a}_{S_x} - \zeta_{I_x}^* \hat{a}_{I_x} - \zeta_{S_y}^* \hat{a}_{S_y} - \zeta_{I_y}^* \hat{a}_{I_y}} e^{\zeta_{S_x} \hat{a}_{S_x}^\dagger + \zeta_{I_x} \hat{a}_{I_x}^\dagger + \zeta_{S_y} \hat{a}_{S_y}^\dagger + \zeta_{I_y} \hat{a}_{I_y}^\dagger} \right] = e^{-(1+\bar{n})(|\zeta_{S_x} + \zeta_{I_x}|^2 + |\zeta_{S_y} + \zeta_{I_y}|^2)/2 - (|\zeta_{S_x} - \zeta_{I_x}|^2 + |\zeta_{S_y} - \zeta_{I_y}|^2)/2 + \bar{n} \text{Re}[(\zeta_{S_x} + \zeta_{I_x})(\zeta_{S_y} + \zeta_{I_y})]}, \quad (4.1)$$

where $\bar{n} \equiv I_- - I_+$ and $\tilde{n} \equiv I_- + I_+$, with $I_{\mp} \equiv \eta_L \gamma \gamma_c G / \Gamma_c (1 \mp G) [(1 \mp G)\Gamma + \Gamma_c]$, as before. Using this density operator, the erasure probability for the degenerate-OPA quantum communication systems is found via,

$$P_{\text{erasure}} = \left(S_x \langle 0 | S_y \langle 0 | \hat{\rho}_{S_x S_y} | 0 \rangle_{S_y} | 0 \rangle_{S_x} \right) + \left(I_x \langle 0 | I_y \langle 0 | \hat{\rho}_{I_x I_y} | 0 \rangle_{I_y} | 0 \rangle_{I_x} \right) - \left(S_x \langle 0 | I_x \langle 0 | S_y \langle 0 | I_y \langle 0 | \hat{\rho}_{S_x I_x S_y I_y} | 0 \rangle_{I_y} | 0 \rangle_{S_y} | 0 \rangle_{I_x} | 0 \rangle_{S_x} \right), \quad (4.2)$$

its success probability is calculated from $P_{\text{success}} = {}_{SI} \langle \phi | \hat{\rho}_{\vec{S}\vec{I}} | \phi \rangle_{SI}$, and its error probability is obtained from the closure relation, $P_{\text{error}} = 1 - P_{\text{erasure}} - P_{\text{success}}$. Throughput and fidelity

results follow directly from these probabilities and the memory cycling rate, just as they did for the dual-OPA source case that was treated in Sect. III.

Figure 5(a) compares the throughputs of the dual-OPA and the degenerate OPA teleportation systems and Fig. 5(b) shows their loss-limited fidelities when the OPAs are operated at 1% of oscillation threshold, $G^2 = 0.01$, and the loss assumptions are the same as those made for Fig. 3. At this pumping level the dual-OPA source supports a throughput of 200 pairs/sec out to a 50 km end-to-end span with 97.5% fidelity, whereas the degenerate-OPA source achieves only 50 pairs/sec at a slightly lower fidelity over this same span. The 6 dB difference between the dual-OPA and degenerate-OPA throughputs is easily explained. The degenerate-OPA configuration has half the raw flux of the dual-OPA system, because each of the latter's individual OPAs is pumped at 1% of threshold. The degenerate OPA suffers an additional factor-of-two loss, relative to the dual-OPA setup, because of the 50/50 beam splitter in Fig. 4. Specifically, the full flux of the dual-OPA setup is losslessly combined by the polarizing beam splitter in Fig. 2(b), whereas half the time both photons emerge from the same output port of the degenerate-OPA configuration's 50/50 beam splitter thus precluding formation of the triplet state needed for a loading success.

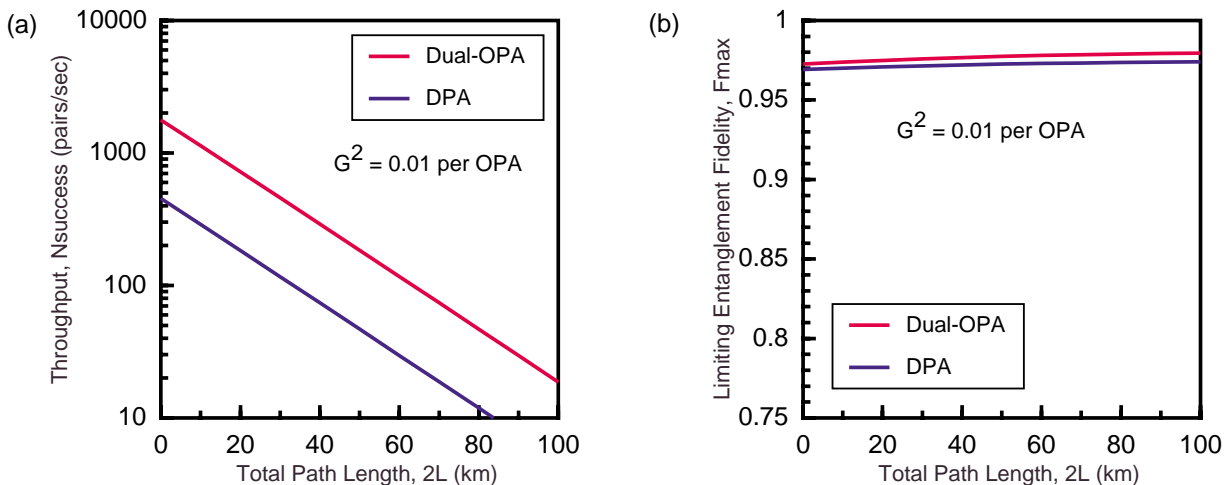


FIG. 5. Teleportation figures of merit for dual-OPA and degenerate parametric amplifier (DPA) source configurations. Left (a), throughput, N_{success} , vs. total path length, $2L$. Right (b), limiting entanglement fidelity, F_{max} , vs. total path length, $2L$. All curves assume OPAs operating at 1% of their oscillation thresholds, 5 dB of excess loss per P -to- M block connection, and 0.2 dB/km fiber-propagation loss.

Comparison of the dual-OPA throughput curve in Fig. 5 with the one shown in Fig. 4 reveals the value of OPA gain optimization: at 50 km total path length, throughput is increased by a factor of four by increasing OPA pumping from 1% to 2.3%. The price paid for this throughput increase is a decrease in fidelity from 97.5% to 95%.

V. GHZ-STATE COMMUNICATION

Singlet-state teleportation relies on two-particle entanglement. There is considerable interest currently in N -party entanglement, i.e., in the generation and application of en-

tangled states of $N > 2$ particles. Greenberger, Horne, and Zeilinger showed that such multi-particle states were of fundamental importance because they led to conflicts with local realism for nonstatistical predictions of quantum mechanics [12]. The simplest state of this Greenberger-Horne-Zeilinger (GHZ) class, viz., $|\psi\rangle_{\text{GHZ}} \equiv (|\uparrow\rangle|\uparrow\rangle|\bullet\rangle + |\bullet\rangle|\bullet\rangle|\uparrow\rangle)/\sqrt{2}$, has been shown, theoretically, to permit quantum secret sharing [13]. The initial experimental demonstration of GHZ-state generation by Bouwmeester *et al.* [4], like their earlier work on singlet-state teleportation, was an annihilative table-top measurement. Moreover it had an extremely low flux: 1 GHZ state every 150 seconds. Here we will show that the MIT/NU quantum communication architecture can lead to long-distance transmission and storage of GHZ states via an alerted detection scheme akin to that in [4].

Figure 6(a) is a simplified redrawing of the Innsbruck group’s GHZ-state source, in which we have replaced their parametric downconverter with a pair of doubly-resonant, type-II phase matched degenerate OPAs—arranged as in Fig. 2(b) to produce polarization entanglement—and we have placed a trapped-atom quantum memory at the trigger-output port of the polarizing beam splitter. Figure 6(b) shows the embedding of this GHZ-state source into a long-distance quantum communication architecture in which L -km-long spans of standard telecommunication fiber are used to connect to trapped-Rb atom quantum memories. (As in Fig. 1, we have not shown the quantum frequency conversion and time-division multiplexing arrangements that are needed to make use of the $1.55\ \mu\text{m}$ low-loss window and to suppress the ill-effects of time-varying birefringence.)

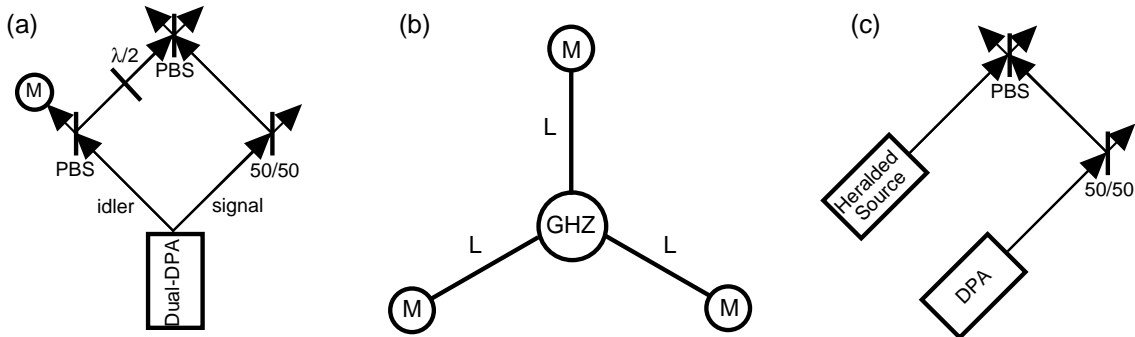


FIG. 6. Left (a), degenerate parametric amplifier system for generation of GHZ states. Dual degenerate parametric amplifier (dual-DPA) is a Fig. 2(b) arrangement in which OPAs 1 and 2 operate at frequency degeneracy and are pumped in phase. PBS polarizing beam splitter; M trapped-Rb atom quantum memory; $\lambda/2$ half-wave plate. Middle (b), Long-distance communication architecture for GHZ states. GHZ is the source arrangement from either (a) or (c); L denotes L km of standard telecommunication fiber. Right (c), heralded single-photon source plus degenerate parametric amplifier system for generation of GHZ states.

The system in Figs. 6(a),(b) is run under a clocked protocol similar to the one described for singlet-state transmission in Sect. III. In each time epoch we monitor the cycling transitions on all four quantum memories, viz., the three external memories shown in Fig. 6(b) plus the fourth memory (internal to the source block in that panel) that is present in Fig. 6(a). The loading protocol is repeated until all four memories absorb photons in the same time epoch.

As shown for annihilative measurements in [4], when all four memories in Figs. 6(a),(b) have absorbed photons, and these photons came from the emission of two entangled signal-idler pairs from the degenerate OPA, then the three external memories have been loaded into a GHZ state.

A throughput and loss-limited fidelity analysis of this GHZ-state communication scheme can be carried out using the OPA and cavity-loading statistics that we have described in Sects. III and IV. Figure 7 shows an example of the results from such an analysis. The lower curves in this figure are the throughput [Fig. 7(a)] and the fidelity [Fig. 7(b)] vs. source-to-memory path length L when the fixed and propagation losses are 5 dB and 0.2 dB/km, respectively, and the normalized OPA gain is $G^2 = 0.005$. [Because the Fig. 6 architecture is not being used for singlet-state teleportation, the fidelity measure we have employed here is the conditional probability that the Fig. 6(b) memories are in the GHZ state, i.e., $F_{\max} = P_{\text{success}}/(P_{\text{success}} + P_{\text{error}})$.] The greatly reduced likelihood that an OPA produces two signal-idler pairs in a loading interval—as compared to its probability of producing one such pair—is the primary reason that the GHZ-state throughput in Fig. 7(a) is so much lower than the teleportation throughputs we saw in Figs. 3(a) and 5(a). On the positive side, however, we see that the architecture from Figs. 6(a),(b) permits a throughput comparable to what Bouwmeester *et al.* produced in the laboratory to be realized over a 10 km source-to-memory radius with a fidelity just under 90%. More important, though, is the fact that the memories in the Fig. 6 architecture allow the GHZ state to be stored for use in quantum secret sharing or other applications of 3-particle entanglement.

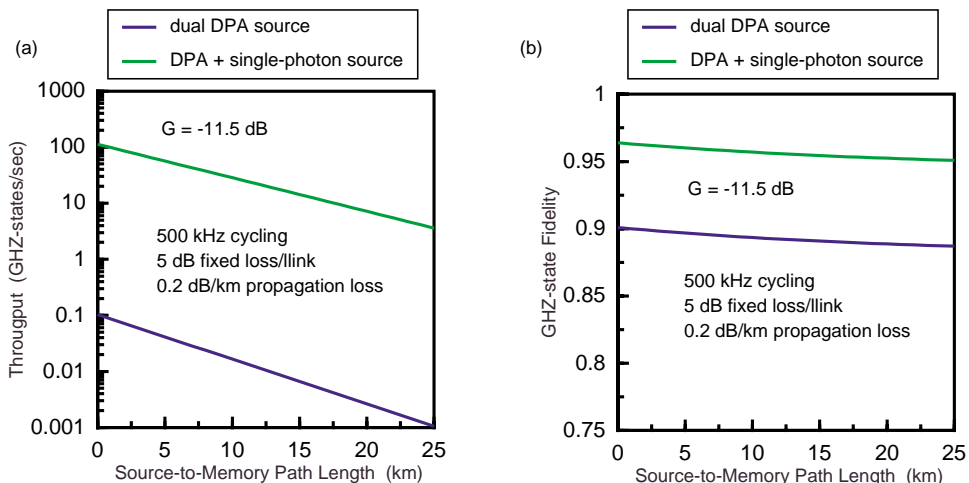


FIG. 7. Figures of merit for the Fig. 6 architecture. Left (a), GHZ-state throughput vs. source-to-memory path length, L , for dual degenerate parametric amplifier (dual-DPA) and DPA plus heralded single-photon sources. Right (b), GHZ-state transmission fidelity vs. source-to-memory path length, L , for dual-DPA and DPA plus heralded single-photon sources. All curves assume 5 dB of excess loss per source-to-memory connection, and 0.2 dB/km fiber-propagation loss.

A route to obtaining substantially higher throughputs from the Fig. 6(b) architecture may be developed by examining the role of the memory element in Fig. 6(a). Suppose

that the dual-DPA emits two entangled-photon pairs from which each of the memories in Figs. 6(a),(b) captures one photon. The polarization of the photon captured by the Fig. 6(a) memory is determined, by the polarizing beam splitter, as is the polarization of the photon entering the half-wave plate in that figure. The half-wave plate’s orientation forces the latter photon to have a 50/50 chance of taking either output port of the ensuing polarizing beam splitter. It then follows that the three external memories share a GHZ state. Note that the sole purpose of the Fig. 6(a) memory is to serve as a trigger, i.e., to herald (by its absorbing a photon of a definite polarization) the presence of a photon in the orthogonal polarization at the input to the half-wave plate. Recent work has shown that it may be possible to construct heralded single-photon sources [14]. With such a source, used in the configuration shown in Fig. 6(c), there would be a single photon entering the half-wave plate during every cycle of the loading protocol, as compared to the much lower flux that prevails in the Fig. 6(a) version of the GHZ-state source. When this heralded source produces one photon per loading interval in the proper spatio-temporal mode for coupling to the trapped-atom quantum memory, vastly improved GHZ-state communication results from using the Fig. 6(c) source in the Fig. 6(b) transmission architecture, as shown by the upper curves in Fig. 7. In particular, throughput rises by three orders of magnitude—to more than 30 GHZ states/sec at 10 km radius—and fidelity increases to more than 95%.

Neither the dual-DPA nor the DPA plus heralded source calculations have been optimized over OPA gain. Moreover, the source-to-memory radius for which GHZ-state communication can be achieved can be extended by teleporting the contents of any or all of the Fig. 6(b) memories using the long-distance teleportation architecture shown in Fig. 1. Thus, it should be possible to share GHZ states over long distances for use in quantum secret sharing or other multi-party entanglement protocols.

VI. DISCUSSION

We have described architectures for long-distance, high-fidelity quantum teleportation and GHZ-state transmission. Because of their nondestructive memory-loading verification, their ultrabright entanglement sources, and their ability to employ the low-loss wavelength window in standard telecommunication fiber, these systems can sustain appreciable throughputs and high fidelities over loss-limited operating ranges well beyond those of previous quantum repeater proposals. Of course, our analysis has neglected additional degradations that may arise from residual phase errors in transmission, imperfect Bell-state measurements, etc., which will reduce achievable fidelities. Nevertheless, the Fig. 1 and Fig. 6 configurations offer substantial promise for bringing quantum communications from conditional demonstrations in the laboratory to viable system implementations.

VII. ACKNOWLEDGMENTS

This research was supported by U.S. Army Research Office Grant DAAD19-00-1-0177 and by National Reconnaissance Office Contract NRO000-00-C0032. The author acknowledges fruitful technical discussions with Phillip Hemmer, Peter Hendrickson, Prem Kumar, Seth Lloyd, Selim Shahriar, Franco Wong, and Horace Yuen.

REFERENCES

- [1] J. H. Shapiro, “Long-distance high-fidelity teleportation using singlet states,” in *Quantum Communication, Measurement, and Computing 3*, O. Hirota and P. Tombesi, eds., (Kluwer, New York, 2001), pp. 367–374.
- [2] J. H. Shapiro and N. C. Wong, “An ultrabright narrowband source of polarization-entangled photon pairs,” *J. Opt. B: Quantum Semiclass. Opt.* **2**, L1–L4 (2000).
- [3] S. Lloyd, M. S. Shahriar, J. H. Shapiro, and P. R. Hemmer, “Long distance, unconditional teleportation of atomic states via complete Bell state measurements,” *Phys. Rev. Lett.* **87**, 167903 (2001).
- [4] D. Bouwmeester, J.-W. Pan, M. Daniell, H. Weinfurter, and A. Zeilinger, “Observation of three-photon Greenberger-Horne-Zeilinger entanglement,” *Phys. Rev. Lett.* **82**, 1345–1349 (1999).
- [5] C. H. Bennett, G. Brassard, C. Crépeau, R. Jozsa, A. Peres, and W. K. Wootters, “Teleporting an unknown quantum state via dual classical and Einstein-Podolsky-Rosen channels,” *Phys. Rev. Lett.* **70** 1895–1899 (1993).
- [6] D. Bouwmeester, J.-W. Pan, K. Mattle, M. Eibl, H. Weinfurter, and A. Zeilinger, “Experimental quantum teleportation,” *Nature* **390** 575–579 (1997).
- [7] D. Bouwmeester, K. Mattle, J.-W. Pan, H. Weinfurter, A. Zeilinger, and M. Zukowski, “Experimental quantum teleportation of arbitrary quantum states,” *Appl. Phys. B* **67** 749–752 (1998).
- [8] P. Kumar, “Quantum frequency conversion,” *Opt. Lett.* **15** 1476–1478 (1990).
- [9] J. M. Huang and P. Kumar, “Observation of quantum frequency conversion,” *Phys. Rev. Lett.* **68** 2153–2156 (1992).
- [10] K. Bergman, C. R. Doerr, H. A. Haus, and M. Shirasaki, “Sub-shot-noise measurement with fiber-squeezed optical pulses,” *Opt. Lett.* **18** 643–645 (1993).
- [11] N. C. Wong, K. W. Leong, and J. H. Shapiro, “Quantum correlation and absorption spectroscopy in an optical parametric oscillator in the presence of pump noise,” *Opt. Lett.* **15**, 891–893 (1990).
- [12] D. M. Greenberger, M. A. Horne, and A. Zeilinger, “Going beyond Bell’s theorem,” in *Bell’s Theorem, Quantum Theory, and Conceptions of the Universe*, M. Kafatos ed. (Kluwer, Dordrecht, 1989), pp. 73–76.
- [13] M. Hillery, V. Buzek, and A. Berthiaume, “Quantum secret sharing,” *Phys. Rev. A* **59**, 1829–1834 (1999).
- [14] C. Santori, M. Pelton, G. Solomon, Y. Dale, and Y. Yamamoto, “Triggered single photons from a quantum dot,” *Phys. Rev. Lett.* **86**, 1502–1505 (2000).